Unconventional fabrication of 2D nanostructures and graphene edges

Bellunato, A.

CHAPTER 1

Introduction

Graphene is a bi-dimensional allotrope of carbon arranged in a monoatomic layer of sp^2 hybridized carbon atoms packed in a honeycomb lattice. The hexagonal pattern of unsaturated atoms yields an extended aromaticity through the lattice formed by the p_z electrons responsible of the π bonds among the carbon atoms. As in conjugated organic semiconductors, the extended conjugation of half-filled p_z orbitals forms π valence and conductance bands. As opposed to σ orbitals, responsible for deep valence bands behind the rigid structure of graphene, π bands present a linear electronic dispersion where the valence and conduction bands meet at the Fermi level[1,2] (Figure 1.1a). π bands are responsible for the intrinsic conductivity of graphene, where electrons promoted to the conduction band by thermal energy or doping can move as massless fermions through the lattice of graphene, at speed up to only 300 times slower than light[3].

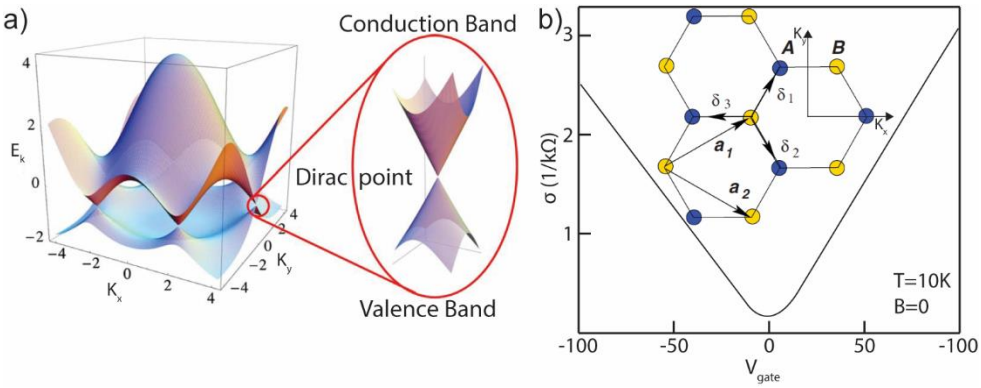

Figure 1.1. Hexagonal honeycomb lattice of graphene. a) Electronic dispersion in the graphene reciprocal lattice. Inset: magnification on the cone structure at the Dirac point. The two bands meet at the Fermi Level[1]. b) I-V_{gate} characteristic of graphene. Inset: graphene lattice and reciprocal lattice defined by the K vectors[1].

The linear dispersion of the band structure has an immediate effect on the conductivity of graphene[4]. External electric fields modulate the electrons population of the conduction band, yielding a gate effect. In practice, the external field promotes electrons from the conduction to the valence band modifying the amount of charge carriers in graphene. Sweeping the gate field from lower potential to higher potential yields an increment of electrons in the conduction band. The conductivity curve of graphene assumes a semi-parabolic shape with a minimum of conductivity at the Dirac point, where the promotion of electrons

caused by the gate field balances the amount of holes at the - so called - charge neutrality point. By increasing further the potential, the promoted electrons overcome the amount of holes, restoring a higher conductivity (Figure 1.1b). In proximity of the charge neutrality point, the conductivity of graphene varies exponentially with the electric field, becoming extremely sensitive to field variations (while assuming a linear behaviour far apart of the charge neutrality point).

Similar to a gate field, the interaction between molecules and the surface of graphene results in a direct perturbation of the electronic band structure of graphene. Thus, thanks to the 2D nature of graphene, short-range interactions induced by charges such as dipoles or ions change the electronic band structure of graphene, therefore modulating the electron density populating the valence and conduction bands of graphene[5]. As a result, the conductivity of graphene is modified by the proximity of external perturbations such as adsorbed molecules. Similarly, the chemical functionalization of graphene locally alters the honeycomb lattice of sp^2 hybridized carbon atoms. The introduction of sp^3 defects corresponds to the addition of scattering centres perturbing the motion of the electrons, permanently altering the electronic structure of graphene, changing its conductivity and its entire band-structure. Nonetheless, the widespread sp^2 conjugation results in a relative chemical stability of the carbon atoms composing the lattice of graphene, yielding sensors of high sensitivity, but extremely poor selectivity.

Carbon atoms on the edge of graphene represent a singularity. In fact, these atoms are already located on ruptures of the lattice of graphene, introducing scattering and perturbations in the band structure of graphene. The chemistry at the edges alters the composition of such carbon atoms via functionalization and elemental substitution. Nonetheless, these modifications influence sp^3 carbons intrinsically present in the graphene, without additional damage on the basal plane. Ideally, selectivity can then be achieved without perturbing the physical properties of the basal plane (i.e. sensitivity). At the nanoscale, also, the increased ratio of edge atoms over basal plane atoms leads to a confinement of the aromatic structure of graphene[6]. Edge defects and their chemistry become predominant in the electrodynamics of graphene, modulating directly chemical and physical properties[7–16], such as chemical reactivity and electronic band structure.

The electrical responsiveness of graphene permits its integration as an active element within sensing devices. The atomic thickness and the relative chemical stability, also, offer further advantages in the design of sensors working at the molecular scale, ranging from DNA sequencers[17] to ultra-fast transistors for consumable electronics[4,18]. These, particularly, require the sculpting of graphene into complex architecture with nanometric and sub nanometric precision. Nanoribbons, nanopores and nanogaps form (bio)-sensing platforms relying on precisely patterned graphene nanostructures. The scalable nanoengineering of graphene, though, remains among the biggest challenges of graphene nanotechnology. Conventionally, the controlled sculpting of graphene distinguishes between bottom-up or top-down approaches.

The former assembles graphene nanostructures via the polymerization of polycyclic aromatic hydrocarbons[19]. Particularly, bottom-up techniques grow atomically tailored graphene nanostructures as narrow as a few carbon atoms with chemically designed edges, as explained in more details in Chapter 2. Nevertheless, bottom-up solution synthesis face solubility constrains, with severe issues toward device integration, which limit both the achievable size of the graphene samples and their application[20]. From the aspect of the chemical functionalization of graphene edges, chemical synthesis allows the control of crystallinity, purity, molecular structure and chemical functionality of the edge. Notably, some reports attempted the selective synthesis over pre-patterned substrates[21,22], allowing a precise alignment of the nanostructures over the substrate, but still requiring complex lithographic pre-treatments severely affecting its applicability.

Alternatively, top-down approaches narrow large area graphene films into nanostructures via selective etching of graphene protected underneath a mask. Electron beam lithography[23], either in the form of patterning through a resist or resist-free lithography via transmission electron microscopy, remains the method of choice for the top-down sculpting of graphene nanoarchitectures. Conventionally, electron beam lithography writes a pattern into a polymeric resist coating the graphene[23]. Chain scission occurs in the exposed regions of the *positive* resist yielding a significant change of its solubility into selected solvents, or developer. After the dissolution of the exposed resist, the remaining pattern acts as a mask over the surface of the graphene, while the unprotected graphene areas are further etched in harsh chemical environments such as reactive ion etching,

RIE. At last, the protecting resist is dissolved uncovering the graphene nanostructure. Beam lithography is used for the patterning of graphene nanoribbons as thin as ~10 nm[24]. Furthermore, it is used for the design of nanoconstrictions successively converted into nanogaps[25] for instance via electroburning[26]. Importantly, polymeric resists, organic solvents and harsh ion etching contribute to the contamination of the graphene nanostructures, and affect the composition and the topography of the edges in an uncontrolled manner[27]. Alternatively, transmission electron microscopes, TEM, can generate highly focused electron/ion beams capable of directly patterning graphene without any resist. The particle beam knocks out carbon atoms from the lattice by energetic exchange with graphene[28,29] , yielding for instance nanoribbons[30] and nanopores in free-standing graphene[31,32–35] and other two-dimensional materials[36,37], with superior control over the crystallinity and chemical composition of the edges. Conveniently, the final pattern is characterized in situ using the imaging mode of the electron/ion microscopes[38,31]. Despite the great step-forward performed by lithographic systems in the field of graphene nano-patterning, beam lithography remains a time consuming technique, requiring high vacuum and unable of parallel processing.

Aiming to overcome the main limitations of conventional bottom-up and top-down nanofabrications, in this thesis we showcase different powerful approaches for the simple and flexible design of nanopores, nanogaps and nanoribbons architectures and for the selective chemical functionalization of graphene edges, as illustrated in Chapter 3, Chapter 4 and Chapter 5. Furthermore, we employed such approaches to form metallic nanogaps and polymeric nanofluidic channels as presented respectively in Chapter 6 and Chapter 7. We used microtomy to precisely prepare metallic nanorods embedded in polymeric supports which we assembled into nanopores and nanogaps or used as inert mask for the top-down sculpting of graphene nanoribbons, without employing any conventional lithographic step nor clean room facilities.

Whitesides and co-workers were the first to introduce the microtomy of metallic thin films as an alternative route to fabricate and pattern metallic nanostructures[39,40]. Specifically, metallic thin films are grown via evaporation or atomic layer deposition onto flat substrates and further embedded in polymer, generally epoxy resins[41]. The resulting sample is a composite material constituted

of a metallic thin film surrounded by a polymeric matrix. A sharp diamond knife sections the polymer with nanometric precision, below 30 nm, yielding thin polymeric slabs embedding metallic nanostructures, Figure 1.2a. Practically, the knife works as a wedge at the interface with the polymer matrix, initiating a crack through the brittle polymer matrix[41]. The crack controllably propagates few nm ahead of the knife, extending in proportion to the radius of curvature of the knife. The knife slices through the polymer pushing forward the crack propagation, and yielding a thin section of polymer. The polymer operates as a mechanical support for the metallic filler, allowing the precise transfer and manipulation of the slab. The composite sample slides over the knife, which position is controlled by high-precision piezo-actuators. The diamond knife is atomically sharp with a radius of few nanometres (5 nm to 6 nm), yielding highly precise nanometric polymeric slabs.

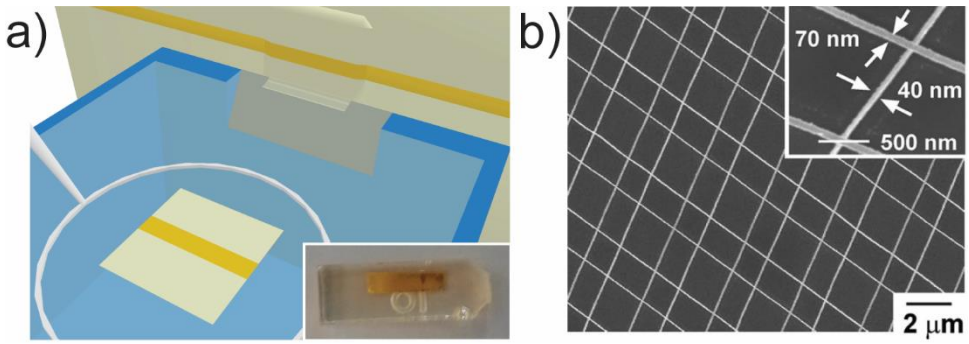

Figure 1.2. Microtomy of nanostructures. a) A diamond knife slices the metallic thin film embedded into the polymer matrix yielding polymeric slabs bearing the metallic nanostructure. Inset: the composite sample formed by a metallic thin film embedded in the polymer matrix. b) Metallic nanorods prepared via microtomy and assembled in complex nano-architectures[39].

The supporting polymer allows the manipulation of the samples and their assembly into suspended and overlapped architectures, Figure 1.2b. Afterwards, the polymer can be removed, leaving in place only the embedding, such as a metallic nanostructure. Alternatively, the metallic embedding can be etched or dissolved, leaving slits into thin polymeric slabs, which can be assembled into nanopores[42], for instance.

In this work, we illustrate the application of microtomy for the sculpting of complex nanostructures with innovative designs. We used microtomy to prepare edges in graphene, first demonstrating their selective chemical functionalization via bulk methods such as electrografting, as illustrated in Chapter 3. Furthermore, the removal of the supporting polymer slab or the metallic embedding resulted in edge tailored graphene nanoribbons with controlled edge chemistry, Chapter 5. By overlapping the slits within two polymeric slabs, we obtained highly precise and mechanically stable zero-depth nanopores, capable of reaching the performances of graphene nanopores, while demonstrating reduced noise, Chapter 7.

1.1 Graphene (bio-)nano-sensors

Graphene showed outstanding initial results in the field of molecular sensing, particularly toward DNA sequencing[33] and single molecule detection[43]. There are several sensing platforms based on graphene[44,45], which rely on multiple working mechanisms, exploiting features such as atomic thickness, mechanical stability and modulated electrical conductivity. These can be divided into three major classes based on diversified working designs and classified as graphene nanopores, graphene field effect transistors (GFET) and nanogaps. Particularly, atomically thin, bidimensional graphene nanopores, ideally, can perform real time DNA sequencing with single nucleotide resolution[46], promoting graphene and bidimensional materials as ideal candidates for the next generation sequencing devices. In the upcoming sections, we will introduce these technologies, their working mechanism, and major challenges, explaining their relevance in the sensing community and shedding a light over the significance of our work.

1.1.1 Graphene nanopores

A nanopore is a nanometric hole drilled in a thin membrane. Molecular sensing in nanopores proceeds by occlusion of the nanopore channel across the membrane[47], Figure 1.3a. In fact, by applying a transmembrane potential within an electrolytic solution, ions move across the hole, yielding a characteristic nanopore conductance G (1):

$$(1)\quad G = \sigma\left[\frac{4L}{\pi d^2} + \frac{1}{d}\right]^{-1}$$

Where σ is the conductivity of the electrolytic solution, L is the length of the nanopore channel and d is the diameter of the pore. Upon molecular translocation, the effective volume of the nanopore decreases, lowering the conductance of the pore. Consequently, despite of a constant transmembrane potential V_{tm}, the electrolytic current intensity across the pore I_p reduces, according to the Ohm's law (2):

$$(2)\quad I_p = V_{tm}G$$

Thus, the overall reduction of the electrolytic current is directly modulated by the size of the translocating molecule[48,49]. The electrolytic current modulation becomes a fingerprint toward molecular recognition and sequencing of DNA strands, particularly single strands, and proteins driven through the pore by the transmembrane potential. In fact, negatively charged single strand DNA molecules are driven through the thread of the pore under the electrostatic force of the same transmembrane potential. Each single nucleotide occludes the pore in an ordered sequence, yielding characteristic dips in the electrolytic current intensity. Afterwards, the sequencing is performed by the analysis of the current dips induced by the molecular translocation[49].

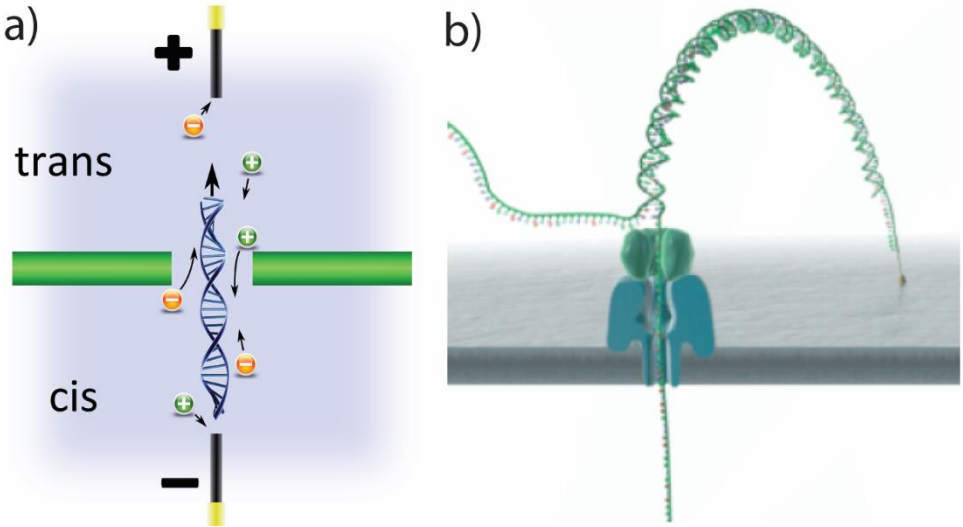

Figure 1.3. Nanopore bio-nanosensors. a) Nanopore working mechanism. A transmembrane voltage (+/-) drives the electrolytes and the analytes through the

pore[50]. b) Schematics of a biological nanopore embedded in a lipidic membrane with an enzyme motor on at its inlet.

The most recent nanopore devices achieved accurate read of long-length DNA single-strands, above 10^3 base pairs. Among these, so called biological nanopores demonstrated outstanding results. Biological nanopores incorporate protein channels such as α-hemolysin into a lipid or polymeric membrane. DNA sequencing happens by translocating the biopolymer through the pore of the protein channel, Figure 1.3b. Biological nanopores can modulate the translocation speed of the DNA single-strands toward a step-like nucleotide translocation which ideally permits single nucleotide resolution with high fidelity. The most effective mechanism to reduce the translocation speed relies on the functionalization of the pore with an enzyme[51], for instance using an enzyme motor such as a DNA polymerase[52–54]. Functionalized biological nanopores modulate the translocation of a single strand DNA, which is driven through the pore by a transmembrane potential. The nanopore modified with an enzyme is now a cheap, portable single strand DNA sequencer currently on the market: the MinION®. It is composed of an array of biological nanopores and is capable of ultra-long reads (> 100 kbp). Interestingly, the enzyme coupled technology allowed the sequencing of 85% of the human genome, corresponding to 2.867 10^6 nucleotides reaching a final read-out accuracy exceeding 99.8%[55]. Importantly, the accuracy achieved via nanopores technologies such as MinION® would have been unreachable without the increasing resolving ability of computational methods, capable of browsing through a dataset composed of around 10^7 bytes of data representative of more than 2 10^6 bases[55]. In fact, while the physical nanopore read-out is still affected by a remarkable mistake (above around 40% on its release in 2014 and reduced below 15% in 2018[56]), the multi-reading process and the analysis algorithm entitle this device of an outstanding reliability[57]. Despite the current commercial success and the dominance of biological nanopores in the landscape of nanopore based DNA sequencers, biological nanopores encounter some limitations. Among these, mechanical fluctuations of the biological membranes majorly affect the performances of such pores. Most importantly, the single nucleotide resolution depends on complex interpretation algorithms, capable of extrapolating sequencing information from the ionic current readings of multiple nucleotides clogging the pore at the same time. In fact, at the thinnest constriction, the pore is around 1,4 nm wide and capable of hosting up to 10 nucleotides in the β-barrel at

the same time, severely modulating the intensity of the ionic current[58]. At last, current technology is single-read, which means that each device can be used once, and needs to be replaced after each read-out.

Alternatively to the current technology, 2D (two-dimensional) materials such as graphene attracted increasing interest for their use in nanopore sequencers. In fact, graphene forms nanopores which channels are atomically thin[31,34] allowing the passage of a single nucleotide per time (Figure 1.4a). Specifically, atomically thin membranes form nanopores which length dimension L is at least one order of magnitude smaller than the diameter d, increasing the overall conductivity of the pore, that becomes $G \propto d$[33]. The ability of a graphene nanopore to detect the passage of a DNA molecule was first demonstrated experimentally in 2010 using a nanopore drilled in a transmission electron microscope, TEM, through a suspended graphene membrane over a SiN support[31]. Figure 1.4b shows the electrolytic current dips relative to translocation events caused by the passage of double stranded DNA through a 22nm wide pore. The sensitivity of the graphene is high enough to distinguish among three different folding configurations of a 16µm long DNA molecule. Ever since, nanopores in graphene have been widely tested and implemented.

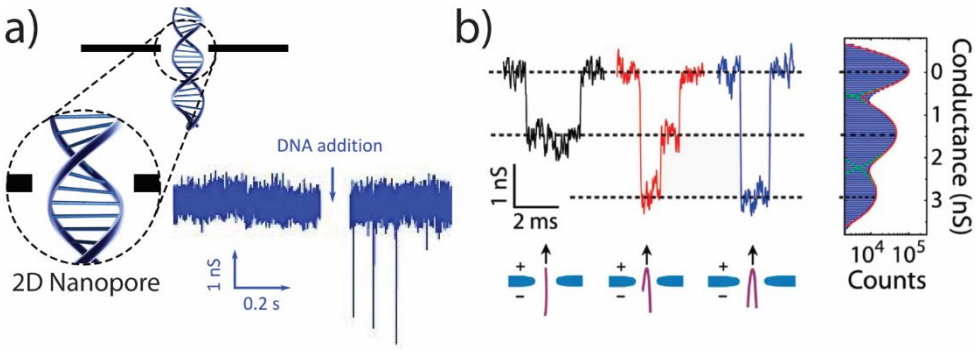

Figure 1.4. Graphene nanopores. a) Top: graphene nanopores translocating a single DNA molecule. Bottom: electrolytic current through a nanopore. The passage of biomolecules such as DNA strands clogs the pore reducing the conductance[31]. b) Differentiation between translocation events in folded and unfolded DNA strands.

Despite the great sensitivity to molecular translocation, graphene based nanopores sequencers are not available yet. The most relevant challenges relate both to the dynamic of translocation, such as the translocation speed, and the intrinsic characteristics of the nanopore, such as the mechanical stability, the hydrophobicity and the - so called - access resistance. The translocation speed is among the most severe limitations[59]. In the case of single stranded lambda DNA, each nucleotide translocates at a rate around 20 ns/nucleotide[31,50], under a transmembrane potential in the order of 100 mV. Consequently, such a translocation speed demands for an acquisition speed above 1 MHz to resolve between the current dips due to the passage of each nucleotide. Additionally, the ions surrounding the membrane form a capacitive coupling with high frequency noise, usually filtered at 10 kHz via a band-pass filter during the current recording[60].

Graphene nanopores (more generally 2D nanopores) have also a low frequency (f) noise[61] that modulates as 1/f and its origin is not yet fully understood, negatively affecting the resolution of the pore. Mechanical fluctuations of the suspended membrane are a possible cause of the 1/f noise. It has been demonstrated experimentally that the noise reduces proportionally to the thickness of the membrane[62], as a consequence of the higher membrane stiffness. Alternatively, shrinking the suspended area of the membrane appears to increase the signal to noise ratio[50].

The transmigration of ions through the pore, also, gives rise to the so called access resistance[63]. When considering the elements composing the conductivity of a nanopore as expressed in equation 1, two components are involved: the channel resistance and the access resistance. The channel resistance stems from the physical passage of ions through the channel composing the pore. The access resistance, on the other hand, relates to a hemisphere around both sides of the mouth of the pore where the concentration of ions increases at the inlet/outlet of the pore. When considering 2D membranes, the channel resistance converges to null. Thus, the access resistance becomes predominant, and the hemispherical volume of ions condensation around the pore represents a so called effective volume of the pore and is directly proportional to the pore diameter, extending over the same nanometer scale. In fact, the condensation of the ions flow already modulates the ionic transport, thus the electrolytic current. Consequently, the hemispheric volume around the mouth of the pore represents an area of reduced

sensitivity of the pore, which loses its ability of distinguishing between different nucleotides within the volume of access resistance, thus losing single nucleotide resolution.

Furthermore, the interaction of molecules such as DNA with the hydrophobic graphene membrane might perturb the translocation through the nanopores[64]. In fact, graphene tends to adsorb irreversibly molecules such as single DNA strands on its surface, hindering the molecular flow. Interestingly, such a drawback is considered often as a starting point to controllably modulate the translocation speed[65]. For instance, exposed graphene nanopores stacked in between two nanopores drilled in aluminium oxide (Al_2O_3) membranes might locally interact with the DNA strand slowing the passage of the strand through the nanopore[66]. Also, the chemical functionalization of the graphene surface might allow a trap-release mechanism, which influences the rate of nucleotides crossing the pore. Nonetheless, while hydrophilic coatings appeared effective in preventing the adsorption of hydrophobic molecules on graphene[67], they also increase the overall thickness of the membrane, thus affecting its resolution abilities.

In conclusion, it is still a technological challenge to achieve molecular sensors, particularly sequencers, based on graphene nanopores or other 2D materials. The advantages introduced by the monoatomic thickness are counterbalanced by obstacles preventing single nucleotide resolution, such as access resistance or translocation speed. Aiming to overcome some of the limitations affecting graphene nanopores, an alternative strategy to assemble subatomic thin nanopores: zero-depth nanopores capillaries, is presented in Chapter 7. These form at the intersection of two slits carved into polymeric thin films prepared via microtomy, showing reduced noise and modulated hydrophobicity and capable of slowing the passage of DNA strands through the pore.

The most important limitation of nanopores remains the indirect detection system. In fact, nanopores do not directly probe molecules. Instead, nanopores extrapolate information from fluctuations in the ionic solution surrounding and interacting with the transmigrating molecule. Indirect characterization has several inherent drawbacks caused directly by the nanopore architecture, for instance mechanical instability or irreversible molecular adsorption.

1.1.2 Graphene field effect transistors

Field effect transistors exploit the modular electronic properties of graphene upon interaction with external stimuli such as molecular adsorption[43,68].

The extended conjugation network of graphene forms a diffused electron distribution that entitles this material of an extremely high charge carrier mobility[69] up to 10^5 cm^2 V^{-1} s^{-1}. The highly regular lattice of carbon atoms and the absence of a layered structure, ideally, yields massless fermion-like electrons moving unscattered over the surface of graphene, and arranged within a conical semi-metallic band structure with 0 eV bandgap[70,71].These mobile electrons can be perturbed under the effect of an external field, modulating the conductivity of the film.

In a transistor configuration, graphene is connected via a source and a drain electrode, while an external field is applied in the form of a gate voltage, either through an electrolytic solution, for instance KCl, or through a capacitive substrate such as SiO_2[72]. Sweeping the gate voltage returns a cone-shaped conductance characteristic of graphene and with a minimum of conductance at the so called Dirac point, or charge neutrality point, Figure 1.5a. The cone-shaped conductance curve offers interesting features for sensing applications. In fact, the interaction between graphene and molecules locally perturbs the electronic band structure of graphene, operating a shift of its Dirac point. Covalent bonds[73–75] and non-covalent interactions[76–78] such as van der Waals, dipoles and π-π stacking modulate the conductivity of graphene, shifting the position of its Dirac point and the amplitude of the cone-shaped conductance curve. The induced variation in conductance works as the sensing fingerprint. Importantly, the cone-shaped conductance curve is steep around the Dirac-point where it follows a parabolic trend. Thus, sensing at the Dirac point returns highly responsive sensors, where small perturbations have a significant impact on the overall conductivity of graphene. This yielded sensors capable of detecting molecules dispersed in extremely low concentrations[72], up to a single molecule physisorbed on the surface of a graphene transistor[43,79].

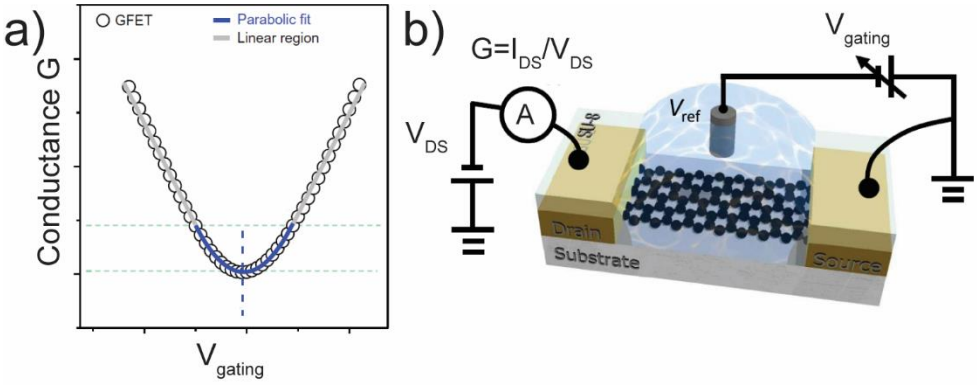

Figure 1.5. Graphene field effect transistor. a) Conductivity curve of graphene under the effect of an external electric field: the gate voltage modulates the conductance of graphene with a minimum of conductance at the Dirac point. b) Liquid gated GFET. A potential is applied between the source and drain electrode of graphene, while the gate potential is applied through an electrolytic solution (blue droplet), modulating the conductance of graphene[80].

Similarly, a gate potential can be applied by means of a reference electrode immersed in an electrolytic solution[81], a process so called liquid gating. Ideally, the electrolyte works as a dielectric causing the potential fall between the electrode and the graphene, Figure 1.5b. The ions of the electrolyte move both toward the surface of the electrode and the surface of graphene. The local charging of the graphene surface attracts immediately oppositely charged ions which counterbalance the potential fall across the solution via the formation of an electrical insulating double layer[82,83]. The field developing across the double layer, then, works as the gating source of the graphene. Liquid gating is an interesting feature of graphene for molecular sensing, as it allows to integrate graphene transistors within fluidic channels and to dissolve analytes into the electrolytic solution. Sensing is based on the local charge perturbation induced by the interaction between the graphene and the molecule. This causes a shift of the Dirac point position resulting in a change in conductance of the liquid gated graphene transistor[82].

Graphene transistors are primarily responsive to charge distributions carried by the molecules. Complex analytes composed of several molecular species might induce non-selective sensing responses. Accordingly, the selectivity of the

transistor can be increased by chemical functionalization of the graphene[82]. Covalent functionalization introduces target receptors chemically bound to the honeycomb lattice of graphene. The resulting chemical bond in graphene induces a sp^2 to sp^3 re-hybridization of the carbon atoms composing the lattice of graphene[84]. This introduces defects in the conjugation network of the honeycomb lattice of graphene, yielding local scattering centres affecting the conductivity of graphene[85]. The overall effect is a reduction of the conductivity and flattening of the Dirac cone, leading to a higher selectivity at the cost of a lower sensitivity.

Alternatively, non-covalent functionalization absorbs selective receptors on the surface of graphene via short range interactions, such as π-π stacking, van der Waals and electrostatic forces[86–88]. For instance, single stranded DNA was immobilized on graphene field effect transistors via non covalent adsorption of biotinylated bovine serum albumin[89] which immobilize DNA via biotin–streptavidin-binding. These were then capable of detecting the immobilization and hybridization of complementary DNA with concentration as low as 100 fM. Interestingly, it was also demonstrated the ability of a graphene field effect transistor, GFET, to distinguish between the adsorption of the four different nucleotides[90].

Particularly, GFET composed of graphene nanoribbons have shown promising theoretical results toward DNA sequencing. Graphene nanoribbons, nanometric thin strips of graphene, compose GFETs embedded within nanofluidic channels capable of stretching DNA strands for sequencing. In a first attempt, a nanopore was drilled through a nanoribbon[35,91], Figure 1.6a. During the translocation of each nucleotide through the pore, the local charge density fluctuation provokes a shift in the conductivity of the ribbon, which is recorded along with the electrolytic current. Theoretical calculations demonstrated that the specific conformation of DNA nucleotides lead to specific charge fluctuations and were proposed for sequencing applications. As an alternative configuration, a GFET composed of a nanoribbon over a nanofluidic channel[92], Figure 1.6b, was also proposed for DNA sequencing. Here, the DNA temporarily adsorbs onto the graphene via π-π stacking modulating the conductance of graphene. In the meantime, a trans-channel potential pushes further the DNA strand. Accordingly to the molecular dynamics, MD, simulations the conductivity of graphene varies as a function of the gate potential as $G(V_g)$[92]:

$$(3)\quad G(V_g) = \frac{2e^2}{h} T(\mu)$$

Where h is the Planck's constant, e the elementary charge and T the transmission curve of the graphene nanoribbon as a function of the chemical potential $\mu(V_g)=E_F - V_g$, with E_F that is the Fermi Level of the graphene ribbon, thus (3) becomes:

$$(4)\quad G(V_g) = \frac{2e^2}{h} T(E_F - V_g)$$

In order to retain the most detailed sequencing information the model demands for a scan over the gating potential to characterize the conductance curve during the interaction of graphene with each nucleotide. These requirements showcase once more the problem related to the translocations speed, which also in case of sweeping frequency in the order of 10 Mhz, would still impose a flow rate of the DNA strand in the order of 0.1 µs per nucleotide.

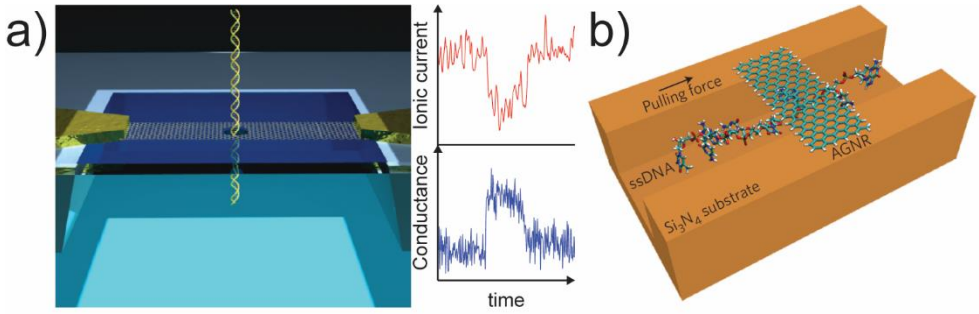

Figure 1.6. Graphene field effect transistors, GFETS, DNA sequencers. a) Left: schematics of a DNA molecule translocating through a nanopore drilled through a GFET nanoribbon. Right: upon the passage of a DNA strand, the ionic current through the nanopore reduces, while the electronic perturbation of the graphene rises its conductance[35]. b) A GFET nanoribbon bridging a nanochannel. The pulling force is the electric field leading the DNA molecule through the channel[92].

Practically, the extremely fast passage of DNA strands allows to identify the resistive variation of the graphene ribbon, nonetheless without achieving single nucleotide resolution. An ideal solution would be the chemical design of highly selective graphene transistors capable of modulating the interaction with DNA strands, but without affecting the electrical properties of graphene. As a result, there is an increasing interest in the chemical functionalization of the edges of

graphene. It is expected that highly reactive edges can precisely modulate the functionality of graphene without lowering the conjugation degree of the honeycomb lattice thus the electronic properties of graphene.

Notably, important steps forward were made recently. Particularly, Heerema et al.[93] successfully drilled a nanopore through a nanoribbon, and managed to design an electronic acquisition system capable of detecting the resistive response of graphene upon interaction with DNA molecules. Even if the carefully designed electronics manages to drastically reduce many capacity elements detrimental for the measurement, the approach remains too challenging. Indeed, they reported the severe unreliability of the device, due to the complex, multistep nanofabrications with a high failure rate, stressing the need of alternative fabrication methods than conventional lithography. Accordingly, Chapter 5 describes the single step fabrication of high aspect ratio graphene nanoribbons, using inert metallic masks fabricated via microtomy instead of lithographically designed polymeric masks.

1.1.3 Graphene nanogaps

Graphene nanogaps comprise two graphene electrodes interfaced at nanometric distance[94,95]. Under the application of a bias potential, a tunnelling current flows between the edges of the contactless electrodes, which intensity decays exponentially with the size of the gap. The gap between the edges of two graphene layers yields a nanogap composed of atomically thin electrodes. Therefore, graphene nanogaps exploit both the atomic thickness and the electrical properties of graphene.

Ideally, molecular sensing with nanogaps employs transverse tunnelling currents transmitted through the molecule crossing the gap[96–99], Figure 1.7a. The atomic thickness of the electrode ensures the single molecule resolution of the sensing nanogap. In 2010 Postma proposed a theoretical model for DNA sequencing across a graphene nanogap[100]. In principle, fixing the gap size, the transmission probability of each nucleotide yields a tunnelling current used as a sequencing fingerprint. The current varies according to equation (5):

$$(5)\quad I(V, x_0) = \sum_{i=1}^{N} I_0^{B_i}(V) e^{-2k\sqrt{d^2+(x_i-x_0)^2}}$$

Where $I_0^{B_i}$ transverse tunnelling current for the nucleotide "I" along the backbone, V is the bias voltage across the gap, k is the decay constant of the tunnelling current across the gap and function of the gap size, d is the gap size and x_i is the position of the crossing nucleotide with respect the intersecting plane of the gap.

Even though each nucleotide, due to its chemical and structural unicity, is expected to deliver an individual tunnelling intensity, conformational modifications in terms of orientation and distance from the gap electrodes might affect the electron transmission probability, thus the current intensity. Different orientations within the gap broaden the tunnelling current associated to each nucleotide[101]. As a result, it is possible to distinguish between two classes of nucleotides such as purines (G, A) and pyrimidines (C, T), based on their size. Theoretically, a more in-depth resolution can be obtained by sweeping the bias voltage across the gap, allowing sequencing resolution. Experimentally[102], the identification of at least three nucleotides was accomplished in a gold nanogap of about 1nm, respectively resolving between thymidine monophosphate TMP, guanosine monophosphate GMP and cytidine monophosphate CMP, Figure 1.7b.

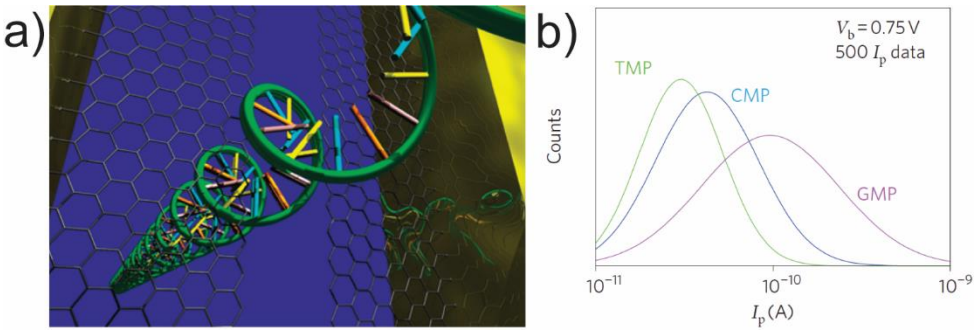

Figure 1.7. DNA sequencing with tunnelling nanogaps. a) Schematics of the sensing mechanisms: a biopolymer passes through the electrodes across the nanogap between the edges of two graphene layers. A bias voltage imposes a tunnelling current which intensity is modulated by the translocating nucleotide[103]. b) Current distributions of TMP, CMP and GMP nucleotides in a gold nanogap of 1nm at V_{bias} = 0.75V[102].

Furthermore, the chemical functionalization of the edges of the graphene electrodes improves the sensing performances of the gap[104]. In fact, theoretical models presented the advantages of hydrogen functionalities on gold electrodes,

promoting the stability of the conduction channels through the nucleotides based on hydrogen-hydrogen interaction[105]. Additionally, the weak bond slows the translocation of the DNA strands through the gap. A similar approach is proposed in graphene, where the controlled chemistry of the edges would stabilize the interactions dynamics between the molecule and the nanogap.

Nonetheless, there is no experimental evidence of DNA sequencing using nanogaps. First, the only current technology available for nanogap sequencing is based on molecular break junctions forming gold atomic contacts[103,106,107]. The resulting gold electrodes lack the atomic thickness of graphene and introduce multiple binding sites for DNA strands, preventing the correct single nucleotide analysis, as explained in Chapter 4. Additionally, the state of the art is the use of supported graphene nanogap, which lack a fluidic system capable of transporting the analytes, introducing a hindering factor for molecular characterization, particularly for sequencing applications.

In Chapter 4, the first dynamic tunnelling junction between independently supported graphene edge electrodes is presented. The formation of a gap between independently supported graphene films interfaced with sub nanometric precision is the first step toward the integration of graphene nanogaps into fluidic systems capable of driving molecules to be directly probed by tunnelling currents. The aim of these experiments is the assessment of a sensing platform able to probe directly the molecules transmigrating through the pore, rather than their influence on the surroundings (as it is in conventional nanopore experimental design). Our results also represent a promising proof of concept for the design of graphene nanogaps integrated into supportive nanopores/nanofluidics architectures. The layered structure of the zero-depth nanopore capillaries (Chapter 7) allows the embodiment of graphene films further converted into independent electrodes reciprocally interfaced across the rim of a pore.

1.2 Aim and outline

In this thesis, we demonstrate unconventional fabrication protocols which differentiate from conventional techniques such as lithography. Particularly, Chapter 2 reports a thorough literature study concerning the state of the art in graphene fabrications toward the selective chemical functionalization of graphene edges. Starting from the literature results, we explored a wide series of

experimental approaches toward the fabrication of graphene bio-sensors with chemically controlled edges, comprising nanopores, nanoribbons and nanogaps architectures. In fact, at the present stage, most of the difficulties relate to extremely complicated fabrication approaches, often based on high resolution electron microscopy or lithography, which severely limits the wide spread of graphene based devices, and the control of the (edge) chemistry.

Accordingly, we investigated the fabrication of edges in graphene, their chemical functionalization and their use as active components at the atomic scale for sensing applications. Particularly, in Chapter 3, microtomy was employed to prepare edges in a graphene transistor embedded in a polymer scaffold, first demonstrating their selective chemical functionalization via bulk methods such as electrografting. In Chapter 4, the first dynamic tunnelling junction between two single carbon atoms at the edge of graphene was prepared via reactive ion etching of a suspended graphene sheet. In Chapter 5, graphene nanoribbons with selectively functionalized edges were formed under the shadowing of a metallic nanorod obtained via microtomy – so called inert mask lithography.

Flexible, unconventional fabrications were employed also in metallic and polymeric materials. Particularly, in Chapter 6 multilayered polyelectrolytes were deposited via Layer-by-Layer deposition between two large area gold films further processed via microtomy into transverse nanogaps between nanorod electrodes. Furthermore, in Chapter 7, we propose a platform that will allow for the first time the integration of graphene electrodes directly within a nanopore, here a nanopore of zero-depth.

Importantly, in our research we tried to preserve the physical integrity of graphene while controlling the chemistry at its edges, with the goal of fabricating reproducible and selective sensors. In this quest, we achieved for the first time the electrochemical functionalization of the edge of a large area graphene monolayer. We overcome the requirements of atomic scale characterizations, clean rooms, and complex designs, targeting a single line of carbon atoms performing experiments at the macroscopic scale and with simple tools available in almost any chemical laboratory.

1.3 References

(1) Castro Neto, a. H.; Peres, N. M. R.; Novoselov, K. S.; Geim, a. K. *Rev. Mod. Phys.* **2009**, *81* (1), 109–162.

(2) Georgakilas, V.; Otyepka, M.; Bourlinos, A. B.; Chandra, V.; Kim, N.; Kemp, K. C.; Hobza, P.; Zboril, R.; Kim, K. S. *Chem. Rev.* **2012**, *112* (11), 6156–6214.

(3) Enoki, T.; Andō, T. *Physics and chemistry of graphene : graphene to nanographene, CRC Press,* **2013**.

(4) Schwierz, F. *Nat. Nanotechnol.* **2010**, *5* (7), 487.

(5) Jiang, D.; Chen, Z. *Graphene Chemistry: Theoretical Perspectives*; Wiley, **2013**.

(6) Baldoni, M.; Sgamellotti, A.; Mercuri, F. *Chem. Phys. Lett.* **2008**, *464* (4–6), 202–207.

(7) Lu, Y. H.; Wu, R. Q.; Shen, L.; Yang, M.; Sha, Z. D.; Cai, Y. Q.; He, P. M.; Feng, Y. P. *Appl. Phys. Lett.* **2009**, *94* (12), 122111.

(8) Simbeck, A. J.; Gu, D.; Kharche, N.; Satyam, P. V.; Avouris, P.; Nayak, S. K. *Phys. Rev. B* **2013**, *88* (3), 35413.

(9) Ohtsuka, M.; Fujii, S.; Kiguchi, M.; Enoki, T. *ACS Nano* **2013**, *7* (8), 6868–6874.

(10) Cervantes-Sodi, F.; Csányi, G.; Piscanec, S.; Ferrari, A. *Phys. Rev. B* **2008**, *77* (16), 165427.

(11) Lee, G.; Cho, K. *Phys. Rev. B* **2009**, *79* (16), 165440.

(12) Hod, O.; Barone, V.; Peralta, J. E.; Scuseria, G. E. *Nano Lett.* **2007**, *7* (8), 2295–2299.

(13) Radovic, L. R.; Bockrath, B. *J. Am. Chem. Soc.* **2005**, *127* (16), 5917–5927.

(14) Seitsonen, A. P.; Saitta, a. M.; Wassmann, T.; Lazzeri, M.; Mauri, F. *Phys. Rev. B* **2010**, *82* (11), 115425.

(15) Jiang, D.; Sumpter, B. G.; Dai, S. *J. Chem. Phys.* **2007**, *126* (13), 134701.

(16) Qi, Z. J.; Rodríguez-Manzo, J. A.; Botello-Méndez, A. R.; Hong, S. J.; Stach, E.

A.; Park, Y. W.; Charlier, J.-C.; Drndić, M.; Johnson, A. T. C. *Nano Lett.* **2014**, *14* (8), 4238–4244.

(17) Heerema, S. J.; Dekker, C. *Nat. Nanotechnol.* **2016**, *11* (2), 127–136.

(18) Zhan, B.; Li, C.; Yang, J.; Jenkins, G.; Huang, W.; Dong, X. *Small* **2014**, *10* (20).

(19) Cai, J.; Ruffieux, P.; Jaafar, R.; Bieri, M.; Braun, T.; Blankenburg, S.; Fasel, R.; Muoth, M.; Seitsonen, A. P.; Saleh, M.; Feng, X.; Mu, K.; Müllen, K. *Nature* **2010**, *466* (7305), 470–473.

(20) Xu, W.; Lee, T.-W. *Mater. Horizons* **2016**, *3* (3), 186–207.

(21) Yu, W. J.; Chae, S. H.; Perello, D.; Lee, S. Y.; Han, G. H.; Yun, M.; Lee, Y. H. *ACS Nano* **2010**, *4* (9), 5480–5486.

(22) Kato, T.; Hatakeyama, R. *Nat. Nanotechnol.* **2012**, *7* (10), 651–656.

(23) Zhang, Y.; Kim, P.; Han, M. Y.; Barbaros, O.; Özyilmaz, B.; Zhang, Y.; Kim, P. *Phys. Rev. Lett.* **2007**, *98* (20), 206805.

(24) Zhang, Y.; Tan, Y.-W.; Stormer, H. L.; Kim, P. *Nature* **2005**, *438* (7065), 201–204.

(25) Wang, H. M.; Zheng, Z.; Wang, Y. Y.; Qiu, J. J.; Guo, Z. B.; Shen, Z. X.; Yu, T. *Appl. Phys. Lett.* **2010**, *96* (2), 23106.

(26) Ullmann, K.; Coto, P. B.; Leitherer, S.; Molina-Ontoria, A.; MartIn, N.; Thoss, M.; Weber, H. B. *Nano Lett.* **2015**, *15* (5), 3512–3518.

(27) Bellunato, A.; Arjmandi Tash, H.; Cesa, Y.; Schneider, G. F. *ChemPhysChem* **2016**, *17* (6), 785–801.

(28) Smith, B. W.; Luzzi, D. E. *J. Appl. Phys.* **2001**, *90* (7), 3509.

(29) Girit, C. O.; Meyer, J. C.; Erni, R.; Rossell, M. D.; Kisielowski, C.; Yang, L.; Park, C.-H.; Crommie, M. F.; Cohen, M. L.; Louie, S. G.; Zettl, A. *Science.* **2009**, *323* (5922), 1705–1708.

(30) Qi, Z. J.; Rodríguez-Manzo, J. a; Botello-Méndez, A. R.; Hong, S. J.; Stach, E. a; Park, Y. W.; Charlier, J.-C.; Drndić, M.; Johnson, a T. C. *Nano Lett.* **2014**.

(31) Schneider, G. F.; Kowalczyk, S. W.; Calado, V. E.; Pandraud, G.; Zandbergen, H. W.; Vandersypen, L. M. K.; Dekker, C. *Nano Lett.* **2010**, *10* (8), 3163–3167.

(32) Fischbein, M. D.; Drndić, M. *Appl. Phys. Lett.* **2008**, *93* (11), 113107.

(33) Merchant, C. A.; Healy, K.; Wanunu, M.; Ray, V.; Peterman, N.; Bartel, J.; Fischbein, M. D.; Venta, K.; Luo, Z.; Johnson, A. T. C.; Drndić, M.; et al. *Nano Lett.* **2010**, *10* (8), 2915–2921.

(34) Garaj, S.; Hubbard, W.; Reina, A.; Kong, J.; Branton, D.; Golovchenko, J. a. *Nature* **2010**, *467* (7312), 190–193.

(35) Traversi, F.; Raillon, C.; Benameur, S. M.; Liu, K.; Khlybov, S.; Tosun, M.; Krasnozhon, D.; Kis, A.; Radenovic, A. *Nat. Nanotechnol.* **2013**, *8* (12), 939–945.

(36) Liu, K.; Feng, J.; Kis, A.; Radenovic, A. *ACS Nano* **2014**, *8* (3), 2504–2511.

(37) Liu, S.; Lu, B.; Zhao, Q.; Li, J.; Gao, T.; Chen, Y.; Zhang, Y.; Liu, Z.; Fan, Z.; Yang, F.; You, L.; Yu, D. *Adv. Mater.* **2013**, *25*, 4549–4554.

(38) Schneider, F.; Houben, L.; Malladi, S. K.; Dekker, C.; Xu, Q.; Wu, M.-Y.; Schneider, G. F.; Houben, L.; Malladi, S. K.; Dekker, C.; Yucelen, E.; Dunin-Borkowski, R. E.; Zandbergen, H. W. *ACS Nano* **2013**, *7* (2), 1566–1572.

(39) Xu, Q.; Rioux, R. M.; Dickey, M. D.; Whitesides, G. M. *Acc. Chem. Res.* **2008**, *41* (12), 1566–1577.

(40) Oomen, P. E.; Zhang, Y.; Chiechi, R. C.; Verpoorte, E.; Mathwig, K. *Lab Chip* **2018**.

(41) Lipomi, D. J.; Martinez, R. V; Rioux, R. M.; Cademartiri, L.; Reus, W. F.; Whitesides, G. M. *ACS Appl. Mater. Interfaces* **2010**, *2* (9), 2503–2514.

(42) Arjmandi-Tash, H.; Bellunato, A.; Wen, C.; Olsthoorn, R. C.; Scheicher, R. H.; Zhang, S.-L.; Schneider, G. F. *Adv. Mater.* **2017**, 1703602.

(43) Schedin, F.; Geim, a K.; Morozov, S. V; Hill, E. W.; Blake, P.; Katsnelson, M. I.; Novoselov, K. S.; F. Schedin A.K. Geim, S. V. M. E. W. H. P. B. M. I. K. & K. S. N. *Nat. Mater.* **2007**, *6* (9), 652–655.

(44) Liu, Y.; Dong, X.; Chen, P. *Chem. Soc. Rev.* **2012**, *41* (6), 2283–2307.

(45) Morales-Narváez, E.; Baptista-Pires, L.; Zamora-Gálvez, A.; Merkoçi, A. *Adv. Mater.* **2017**, *29* (7), 1604905.

(46) Drndić, M. *Nat. Nanotechnol.* **2014**, *9* (10), 743.

(47) Edel, J. B.; Albrecht, T. *Engineered Nanopores for Bioanalytical Applications*; William Andrew, 2013.

(48) Deamer, D. W.; Akeson, M. *Trends Biotechnol.* **2000**, *18* (4), 147–151.

(49) Schneider, G. F.; Dekker, C. *Nat. Biotechnol.* **2012**, *30* (4), 326–328.

(50) Garaj, S.; Liu, S.; Golovchenko, J. A.; Branton, D. *Proc. Natl. Acad. Sci. U. S. A.* **2013**, *110* (30), 12192–12196.

(51) Deamer, D. *Annu. Rev. Biophys.* **2010**, *39* (1), 79–90.

(52) Lieberman, K. R.; Cherf, G. M.; Doody, M. J.; Olasagasti, F.; Kolodji, Y.; Akeson, M. *J. Am. Chem. Soc.* **2010**, *132* (50), 17961–17972.

(53) Cockroft, S. L.; Chu, J.; Amorin, M.; Ghadiri, M. R. *J. Am. Chem. Soc.* **2008**, *130* (3), 818–820.

(54) Sánchez-Quesada, J.; Saghatelian, A.; Cheley, S.; Bayley, H.; Ghadiri, M. R. *Angew. Chemie Int. Ed.* **2004**, *43* (23), 3063–3067.

(55) Jain, M.; Koren, S.; Miga, K. H.; Quick, J.; Rand, A. C.; Sasani, T. A.; Tyson, J. R.; Beggs, A. D.; Dilthey, A. T.; Fiddes, I. T.; Malla, S.; Marriott, H.; Nieto, T.; O'Grady, J.; Olsen, H. E.; Pedersen, B. S.; Rhie, A.; Richardson, H.; Quinlan, A. R.; Snutch, T. P.; Tee, L.; Paten, B.; Phillippy, A. M.; Simpson, J. T.; Loman, N. J.; Loose, M. *Nat. Biotechnol.* **2018**, *36* (4), 338–345.

(56) Rang, F. J.; Kloosterman, W. P.; de Ridder, J. *Genome Biol.* **2018**, *19* (1), 90.

(57) Jansen, H. J.; Liem, M.; Jong-Raadsen, S. A.; Dufour, S.; Weltzien, F.-A.; Swinkels, W.; Koelewijn, A.; Palstra, A. P.; Pelster, B.; Spaink, H. P.; den Thillart, G. E.; Dirks, R. P.; Henkel, C. V. *bioRxiv* **2017**.

(58) Venkatesan, B. M.; Bashir, R. *Nat. Nanotechnol.* **2011**, *6* (10), 615–624.

(59) Arjmandi-Tash, H.; Belyaeva, L. A.; Schneider, G. F. *Chem. Soc. Rev.* **2015**, *45* (3), 476–493.

(60) Wanunu, M. *Phys. Life Rev.* **2012**, *9* (2), 125–158.

(61) Heerema, S. J.; Schneider, G. F.; Rozemuller, M.; Vicarelli, L.; Zandbergen, H. W.; Dekker, C. *Nanotechnology* **2015**, *26* (7), 74001.

(62) Kumar, A.; Park, K.-B.; Kim, H.-M.; Kim, K.-B. *Nanotechnology* **2013**, *24* (49),

495503.

(63) Hall, J. R. *J. Gen. Physiol.* **1975**, *66* (2), 531–532.

(64) Wells, D. B.; Belkin, M.; Comer, J.; Aksimentiev, A. *Nano Lett.* **2012**, *12* (8), 4117–4123.

(65) Sathe, C.; Zou, X.; Leburton, J.-P.; Schulten, K. *ACS Nano* **2011**, *5* (11), 8842–8851.

(66) Kowalczyk, S. W.; Wells, D. B.; Aksimentiev, A.; Dekker, C. *Nano Lett.* **2012**, *12* (2), 1038–1044.

(67) Schneider, G. F.; Xu, Q.; Hage, S.; Luik, S.; Spoor, J. N. H.; Malladi, S.; Zandbergen, H.; Dekker, C. *Nat. Commun.* **2013**, *4*, 2619.

(68) He, Q.; Wu, S.; Yin, Z.; Zhang, H. *Chem. Sci.* **2012**, *3* (6), 1764.

(69) Novoselov, K. S.; Geim, A. K.; Morozov, S. V; Jiang, D.; Zhang, Y.; Dubonos, S. V; Grigorieva, I. V; Firsov, A. A. *Science* **2004**, *306* (5696), 666–669.

(70) Geim, A. K.; Novoselov, K. S. *Nat. Mater.* **2007**, *6*, 183.

(71) Das Sarma, S.; Adam, S.; Hwang, E. H.; Rossi, E. *Rev. Mod. Phys.* **2011**, *83* (2), 407–470.

(72) Fu, W.; Jiang, L.; van Geest, E. P.; Lima, L. M. C.; Schneider, G. F. *Adv. Mater.* **2017**, *29* (6), 1603610.

(73) Bekyarova, E.; Itkis, M. E.; Ramesh, P.; Berger, C.; Sprinkle, M.; de Heer, W. A.; Haddon, R. C. *J. Am. Chem. Soc.* **2009**, *131* (4), 1336–1337.

(74) Koehler, F. M.; Luechinger, N. A.; Ziegler, D.; Athanassiou, E. K.; Grass, R. N.; Rossi, A.; Hierold, C.; Stemmer, A.; Stark, W. J. *Angew. Chemie Int. Ed.* **2009**, *48* (1), 224–227.

(75) Fu, W.; Nef, C.; Knopfmacher, O.; Tarasov, A.; Weiss, M.; Calame, M.; Schönenberger, C.; Schönenberger, C. *Nano Lett.* **2011**, *11* (9), 3597–3600.

(76) Zhang, Z.; Huang, H.; Yang, X.; Zang, L. *J. Phys. Chem. Lett.* **2011**, *2* (22), 2897–2905.

(77) Katoch, J.; Kim, S. N.; Kuang, Z.; Farmer, B. L.; Naik, R. R.; Tatulian, S. A.; Ishigami, M. *Nano Lett.* **2012**, *12* (5), 2342–2346.

(78) Cui, Y.; Kim, S. N.; Jones, S. E.; Wissler, L. L.; Naik, R. R.; McAlpine, M. C. *Nano Lett.* **2010**, *10* (11), 4559–4565.

(79) Sun, J.; Muruganathan, M.; Mizuta, H. *Sci. Adv.* **2016**, *2* (4), e1501518–e1501518.

(80) Fu, W.; Feng, L.; Panaitov, G.; Kireev, D.; Mayer, D.; Offenhäusser, A.; Krause, H. J. *Sci. Adv.* **2017**, *3* (10), e1701247.

(81) Fu, W.; Nef, C.; Knopfmacher, O.; Tarasov, A.; Weiss, M.; Calame, M.; Schönenberger, C. *Nano Lett.* **2011**, *11* (9), 3597–3600.

(82) Aguilella, V. M.; Pellicer, J.; Aguilella-Arzo, M. *Langmuir* **1999**, *15* (19), 6156–6162.

(83) Bockris, J. O.; Gileadi, E.; Müller, K. *J. Chem. Phys.* **1966**, *44* (4), 1445–1456.

(84) Sinitskii, A.; Dimiev, A.; Corley, D. A.; Fursina, A. A.; Kosynkin, D. V; Tour, J. M. *ACS Nano* **2010**, *4* (4), 1949–1954.

(85) Niyogi, S.; Bekyarova, E.; Itkis, M. E.; Zhang, H.; Shepperd, K.; Hicks, J.; Sprinkle, M.; Berger, C.; Lau, C. N.; deHeer, W. A.; Conrad, E. H.; Haddon, R. C. *Nano Lett.* **2010**, *10* (10), 4061–4066.

(86) Yan, F.; Zhang, M.; Li, J. *Adv. Healthc. Mater.* **2014**, *3* (3), 313–331.

(87) Dong, X.; Shi, Y.; Huang, W.; Chen, P.; Li, L.-J. *Adv. Mater.* **2010**, *22* (14), 1649–1653.

(88) Mohanty, N.; Berry, V. *Nano Lett.* **2008**, *8* (12), 4469–4476.

(89) Xu, G.; Abbott, J.; Qin, L.; Yeung, K. Y. M.; Song, Y.; Yoon, H.; Kong, J.; Ham, D. *Nat. Commun.* **2014**, *5*, 4866.

(90) Dontschuk, N.; Stacey, A.; Tadich, A.; Rietwyk, K. J.; Schenk, A.; Edmonds, M. T.; Shimoni, O.; Pakes, C. I.; Prawer, S.; Cervenka, J. *Nat. Commun.* **2015**, *6*, 6563.

(91) Paulechka, E.; Wassenaar, T. A.; Kroenlein, K.; Kazakov, A.; Smolyanitsky, A. *Nanoscale* **2016**, *8* (4), 1861–1867.

(92) Min, S. K.; Kim, W. Y.; Cho, Y.; Kim, K. S. *Nat. Nanotechnol.* **2011**, *6* (3), 162–165.

(93) Heerema, S. J.; Vicarelli, L.; Pud, S.; Schouten, R. N.; Zandbergen, H. W.; Dekker, C. *ACS Nano* **2018**, *12* (3), acsnano.7b08635.

(94) Zhang, P. *Sci. Rep.* **2015**, *5* (1), 9826.

(95) Reed, M. A. *Science* **1997**, *278* (5336), 252–254.

(96) Girdhar, A.; Sathe, C.; Schulten, K.; Leburton, J.-P. *Proc. Natl. Acad. Sci. U. S. A.* **2013**, *110* (42), 16748–16753.

(97) Isaeva, O. G.; Katkov, V. L.; Osipov, V. A. *Eur. Phys. J. B* **2014**, *87* (11), 272.

(98) Liang, X.; Chou, S. Y. *Nano Lett.* **2008**, *8* (5), 1472–1476.

(99) Porath, D.; Bezryadin, A.; de Vries, S.; Dekker, C. *Nature* **2000**, *403* (6770), 635–638.

(100) Postma, H. W. C. *Nano Lett.* **2010**, *10* (2), 420–425.

(101) J. Prasongkit, A. Grigoriev, B. Pathak, R. Ahuja and R. H. Scheicher *Nano Lett.*, **2011**, 11(5), 1941–1945.

(102) Tsutsui, M.; Taniguchi, M.; Yokota, K.; Kawai, T. *Nat. Nanotechnol.* **2010**, *5* (4), 286–290.

(103) Ohshiro, T.; Tsutsui, M.; Yokota, K.; Furuhashi, M.; Taniguchi, M.; Kawai, T. *Nat. Nanotechnol.* **2014**, *9* (10), 835–840.

(104) He, Y.; Scheicher, R. H.; Grigoriev, A.; Ahuja, R.; Long, S.; Huo, Z.; Liu, M. *Adv. Funct. Mater.* **2011**, *21* (14), 2674–2679.

(105) He, H.; Scheicher, R. H.; Pandey, R.; Rocha, A. R.; Sanvito, S.; Grigoriev, A.; Ahuja, R.; Kama, S. P. *J. Phys. Chem. C* **2008**, *112* (10), 3456–3459.

(106) Tsutsui, M.; Taniguchi, M.; Kawai, T. *Appl. Phys. Lett.* **2008**, *93* (16), 163115.

(107) Huang, S.; He, J.; Chang, S.; Zhang, P.; Liang, F.; Li, S.; Tuchband, M.; Fuhrmann, A.; Ros, R.; Lindsay, S. *Nat. Nanotechnol.* **2010**, *5* (12), 868–873.